Wigner Flow Reveals Topological Order in Quantum Phase Space Dynamics

Ole Steuernagel,* Dimitris Kakofengitis, and Georg Ritter

School of Physics, Astronomy and Mathematics, University of Hertfordshire, Hatfield AL10 9AB, United Kingdom

(Received 12 August 2012; revised manuscript received 31 October 2012; published 14 January 2013)

The behavior of classical mechanical systems is characterized by their phase portraits, the collections of their trajectories. Heisenberg's uncertainty principle precludes the existence of sharply defined trajectories, which is why traditionally only the time evolution of wave functions is studied in quantum dynamics. These studies are quite insensitive to the underlying structure of quantum phase space dynamics. We identify the flow that is the quantum analog of classical particle flow along phase portrait lines. It reveals hidden features of quantum dynamics and extra complexity. Being constrained by conserved flow winding numbers, it also reveals fundamental topological order in quantum dynamics that has so far gone unnoticed.

DOI: 10.1103/PhysRevLett.110.030401 PACS numbers: 03.65.-w

Phase portraits characterize the time evolution of dynamical systems and are widely used in classical mechanics [1]. For the conservative motion of a single particle, moving in one dimension x under the influence of a static smooth potential $V(x)$ only, the classical Liouville flow in phase space is regular [2] and largely determined by location and nature of its flow stagnation points. Situated on the x axis wherever the potential is force-free (momentum $p = 0$ and $-\partial V/\partial x = 0$), the local flow forms clockwise vortices around stagnation points at minima of the potential, maxima split the flow and therefore lie at the intersections of flow separatrices, saddle points of the potential lead to an elongated saddle flow pattern oriented along the x axis.

Here we investigate the quantum dynamics of bound states of nonharmonic potentials; their quantum phase space flow reveals rich nonclassical features: Dependence of flow on the state of the system [3] leading to directional deviation from classical trajectories [4] and flow reversal [5], time-dependent quantum displacement of classical stagnation points [6], occurrence of additional nonclassical stagnation points (see Fig. 1 below) whose positions change over time [6] (even for conservative systems), and conservation of the flow orientation winding number ω, see Eq. (6) below, carried by all flow stagnation points during all stages of their time evolution—including instances when they split from or merge with other stagnation points.

For a single quantum particle described by a complex time-dependent amplitude function $\psi(x;t)$ the associated quantum analog of classical phase space probability distributions is Wigner's function $W(x,p;t)$ [7,8], with p the particle's momentum. Structurally, W is a Fourier transform of the off-diagonal coherences of the quantum system's density matrix ϱ, i.e.,

$$W(x,p;t) = \frac{1}{\pi\hbar}\int_{-\infty}^{\infty} dy\,\varrho(x+y, x-y;t)e^{(2i/\hbar)py}, \quad (1)$$

where $\hbar = h/(2\pi)$ is Planck's constant. Unlike ψ or ϱ, the Wigner function only assumes real values, but these do become negative [7,9], defying description in terms of classical probability theory [9–11], thus revealing quantum aspects of a system [12].

The time evolution of W can be cast in the form of a flow field $\boldsymbol{J}(x,p;t)$ [13], the Wigner flow [4], which describes the flow of Wigner's quasiprobability density in phase space. It has the two components

$$\boldsymbol{J} = \begin{pmatrix} J_x \\ J_p \end{pmatrix} = \begin{pmatrix} \frac{p}{m} W(x,p;t) \\ -\sum_{l=0}^{\infty} \frac{(i\hbar/2)^{2l}}{(2l+1)!} \frac{\partial^{2l} W(x,p;t)}{\partial p^{2l}} \frac{\partial^{2l+1} V(x)}{\partial x^{2l+1}} \end{pmatrix}, \quad (2)$$

fulfilling Schrödinger's equation which takes the form

$$\frac{\partial W}{\partial t} + \frac{\partial J_x}{\partial x} + \frac{\partial J_p}{\partial p} = 0 \quad (3)$$

of a continuity equation [7]. Thus, Wigner flow is the equivalent of classical Liouville flow, it has, so far, not been studied in great detail [4,13–15].

Nonlocality [3,16] originates both in definition (1) of the Wigner function and the higher derivatives of V occurring in the Wigner flow (2).

The marginals of the Wigner function yield the probability distributions in position $|\psi(x;t)|^2$ and momentum $|\phi(p;t)|^2$; see Fig. 2 and Refs. [7,9,17]. Integrating over the expressions in the continuity equation analogously shows that the marginals of the Wigner flow yield the respective probability currents in x and p

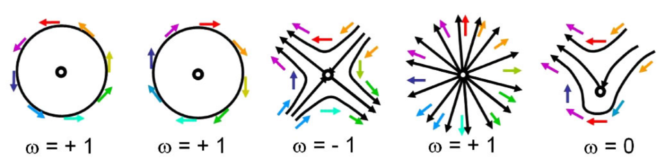

FIG. 1 (color online). Flow field around various types of stagnation points of Wigner flow with associated winding numbers. This list is nonexhaustive.

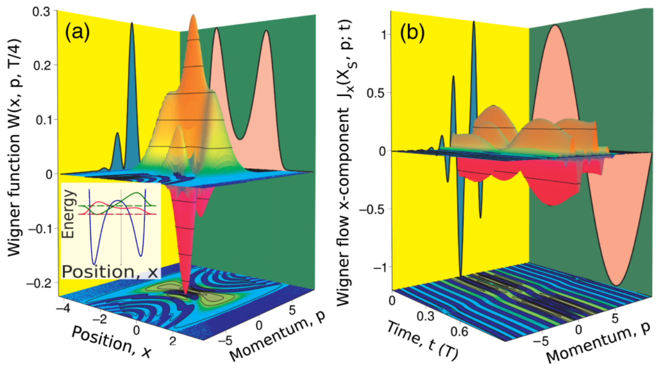

FIG. 2 (color online). Wigner function, Wigner flow, and momentum distribution of state Ψ (parameters $\hbar = 1$, $m = 1/2$, $\alpha = 0.5$, $\Delta E = 0.5$). (a) Wigner function $W(x, p; T/4)$, projection to bottom shows its contours. Projections onto background walls show momentum and position probability distribution (blue and rose filled curves, respectively, in arbitrary units). Inset: Plot of Caticha-potential with wave functions for lowest two energy eigenstates shifted to their respective energy levels (dashed lines). (b) x component of Wigner flow $J_x(X_S, p; t)$ at barrier top at position X_S; bottom projection shows its contours (note its phase shift at $t = T/2$). Projections onto background walls show time and momentum projections (blue and rose filled curves, $\langle J_x(X_S, p)\rangle_T = \int_0^T d\tau J_x(X_S, p; \tau)$ and $\hat{\jmath}_x(X_S; t)$ of Eq. (4), respectively, in arbitrary units). The projection $\hat{\jmath}_x$ features the sinusoidal variation $\propto \sin(2\pi t/T)$ expected of the tunneling current of a two-state system.

$$\frac{d}{dt}|\psi(x;t)^2| = \int_{-\infty}^{\infty} dp J_x(x, p; t) = \hat{\jmath}_x(x;t) \qquad (4)$$

and

$$\frac{d}{dt}|\phi(p;t)^2| = \int_{-\infty}^{\infty} dx J_p(x, p; t) = \hat{\jmath}_p(p;t), \qquad (5)$$

where $\phi(p)$ is the momentum representation of $\psi(x)$. While the x component can be rewritten as the probability current $\hat{\jmath}_x(x;t) = \frac{\hbar}{2im}(\psi^* \partial_x \psi - \psi \partial_x \psi^*)$, in general, no such simple expression exists for $\hat{\jmath}_p(p;t)$.

The dynamics of the harmonic potential, the most studied quantum case, e.g., of quantum optics [9,11], amounts to a rigid rotation of the Wigner function around the origin of phase space. Only at the origin can a flow vortex form (Fig. 3 in Ref. [4]), just like in the classical case. The quantum harmonic oscillator and its isomorphism [18], the free quantum particle [19], constitute exceptional, degenerate cases where lines of stagnation of Wigner flow occur, and not only isolated stagnation points. This is due to the fact that for $V \propto x^2$ or $V =$ const. we have in Eq. (2) $J_p = -W\frac{\partial V}{\partial x}$, just as in the classical limit ($\hbar \to 0$) and, consequently, with $W = 0$ we always find $|\boldsymbol{J}| = 0$. Because of these three facts (rigid rotation, classical form of J_p and line formation) the nonclassical phase space features discussed here cannot be seen in the degenerate cases primarily studied so far [9,11,19].

The degeneracies of the degenerate cases leading to the formation of stagnation lines are lifted for nonharmonic potentials by the presence of terms with $l > 0$ in J_p and leads to the formation of separate stagnation points instead. The boundedness and continuity of wave functions of infinitely differentiable nonharmonic potentials and the unitarity of such systems' quantum dynamics induces homotopies that keep all smooth changes of $\boldsymbol{J}$ in space and time around stagnation points smooth. We therefore conjecture that the topological structure of the Wigner flow field around stagnation points remains conserved. To monitor this we introduce the Wigner flow orientation winding number determined by the integral

$$\omega(\mathcal{L};t) = \frac{1}{2\pi}\oint_{\mathcal{L}} d\varphi \qquad (6)$$

along a closed (convex) loop $\mathcal{L}$; here φ is the orientation angle between the positive x axis and the Wigner flow vectors $\boldsymbol{J}$. For empty paths, not including a stagnation point of $\boldsymbol{J}$, $\omega = 0$; for vortices $\omega = +1$; see Fig 2. The winding number $\omega(\mathcal{L};t)$ is unchanged under continuous path deformations that do not push $\mathcal{L}$ across a stagnation point and as long as time evolution does not move a stagnation point across the loop. It assumes integer values only (assuming the integration path $\mathcal{L}$ does not run through a stagnation point) and is conserved. The sum of winding numbers of all stagnation points within a loop is conserved, even when they split or coalesce: the stagnation points carry topological charge [20].

To give an example, we concentrate on Caticha's [21] smooth, slightly asymmetric, double well potential

$$\begin{aligned} V(x) = {} & 1 + E_0 + \frac{3}{2}\Delta E - \Delta E \alpha \sinh(2x) \\ & + \cosh^2(x)\left(\frac{\Delta E^2}{4}\alpha \sinh(2x) - \frac{\Delta E^2}{4} - 2\Delta E\right) \\ & + \frac{\Delta E^2}{4}(\alpha^2 + 1)\cosh^4(x), \end{aligned} \qquad (7)$$

featuring high outer walls, and wells separated by a barrier of sufficient height, such that at least ground and first excited energy eigenstate tunnel through it; Fig. 2(a) inset. To display all nonclassical flow features listed in the introduction it suffices to investigate the balanced superposition

$$\Psi(x;t) = \frac{\psi_0(x)e^{-iE_0t/\hbar} - \psi_1(x)e^{-i(E_0+\Delta E)t/\hbar}}{\sqrt{2}}, \qquad (8)$$

of ground $\psi_0(x) = \psi_0 \cosh(x) \exp\{-\frac{\Delta E}{4}[\cosh^2(x) + \alpha x + \frac{\alpha}{2}\sinh(2x)]\}$ and first excited state $\psi_1(x) = \psi_1[\alpha + \tanh(x)]\psi_0(x)$, with energies E_0 and $E_0 + \Delta E$ and normalization constants ψ_0 and ψ_1, respectively, [21]. Since the eigenstates are real functions their Wigner functions obey $W(x, p) = W(x, -p)$ which implies that

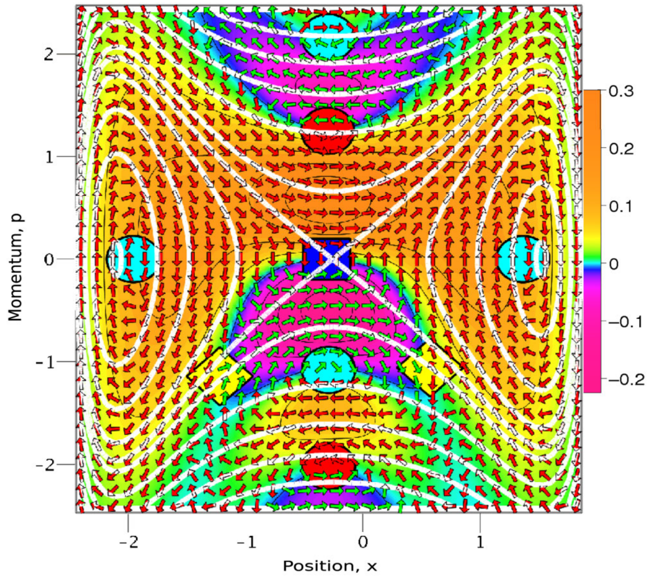

FIG. 3 (color online). Features of Wigner flow of an asymmetric double well potential (same parameters as in Fig. 1, at $t = T/4$). Contour plot of Wigner function $W(x, p; T/4)$ (black contour lines) with an overlay of colored arrows showing normalized Wigner flow $\boldsymbol{J}/|\boldsymbol{J}|$ (red arrows for $W > 0$ and green for $W < 0$). The classical phase portrait is shown as a collection of thick white lines. All locations of Wigner flow stagnation points are highlighted by symbols (cyan and red circles centre on clockwise and anti-clockwise vortices, respectively, yellow diamonds on separatrix intersections, and the blue square on a p-directed saddle flow. The quantum-displacement of the vortices near the potential minima, towards the center, is clearly visible.

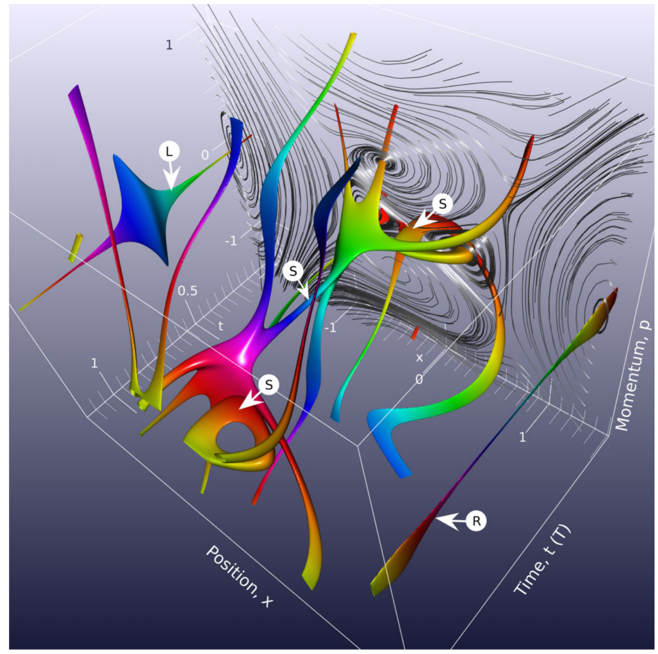

FIG. 4 (color online). Wigner flow's stagnation points' positions across phase space as a function of time. Same parameters as in Fig. 2. The tube surfaces show where in phase space the magnitude of Wigner flow is small $\boldsymbol{J}(x, p; t)^2 = 3 \times 10^{-5}$. They are displayed over 120% of one oscillation period ($t = -0.1T, \ldots, 1.1T$); the rainbow spectrum is matched to T, red-orange for $t = 0$, via green, cyan at $t = 0.5T$, through blue and purple back to red-orange. Because of the periodicity of the two-state scenario, the red-orange-yellow torus is seen twice at the beginning and end of the time window. At the core of all tubes lie time lines of stagnation points. Their movement through phase space leads to their mergers and splits. The gray flow integration lines are guiding the eye past vortices and separatrices, they do not represent physical flow since they integrate $\boldsymbol{J}(x, p; t = 0.05)$ at fixed time. The x coordinate is shown from the left well minimum at $X_L = -2.095$ to the right well minimum at $X_R = 1.514$, the position of the associated vortices ((L) in left well and ® in right), at $p = 0$ and just inside the plot region, confirms the inward quantum-displacement of these stagnation points. The remnant of the classical separatrix stagnation point at position $X_S + \delta x_S(t) \approx -0.3$ is labeled (S). It follows a bent path and becomes displaced, forming part of the torus, when it coalesces with or splits from other stagnation points. All mergers or splits are constrained by topological charge [20] conservation; see Fig. 5.

$$J_x(x, p) = -J_x(x, -p) \tag{9}$$

and

$$J_p(x, p) = J_p(x, -p). \tag{10}$$

Their individual Wigner flow patterns, which the superposition Ψ inherits, are displayed in the Supplemental Material [22]. All these Wigner functions have to be determined numerically [23]. Of the low energy states Ψ is the most dynamic in that it shifts all of the particle's probability distribution back and forth between left and right well. Its Wigner function $W(t = T/4)$ at a quarter of the tunnelling period time ($T = 2\pi\hbar/\Delta E$) is displayed in Figs. 2(a) and 3.

The Wigner flow's state dependence has two aspects: the negativity of W reverses the flow, and the dependence of J_p on W and V leads to sideways deviation of Wigner flow from classical phase portrait lines. In the case of eigenstates of the harmonic oscillator, the former leads to shear flow between neighboring sectors of alternating polarity [4]. The latter deviation can remain mild for eigenstates of a weakly anharmonic potential [4], in our case it is very pronounced leading to the formation of nonclassical vortices which are quantum displaced off the x axis and some of which spin anticlockwise, Figs. 1 and 3. Indications of nonclassical vortices seem to have been observed in chaotic quantum systems before [24].

Flow reversal affects quantum tunneling. The wave function of a particle, tunneling through a barrier, is coherent across it, implying that interference fringes of the Wigner function form in the tunneling region; orientated parallel to the x axis [10], Figs. 2(b) and 3. Neighboring phase space regions contain strips of alternating Wigner function polarity alternating their flow direction [6],

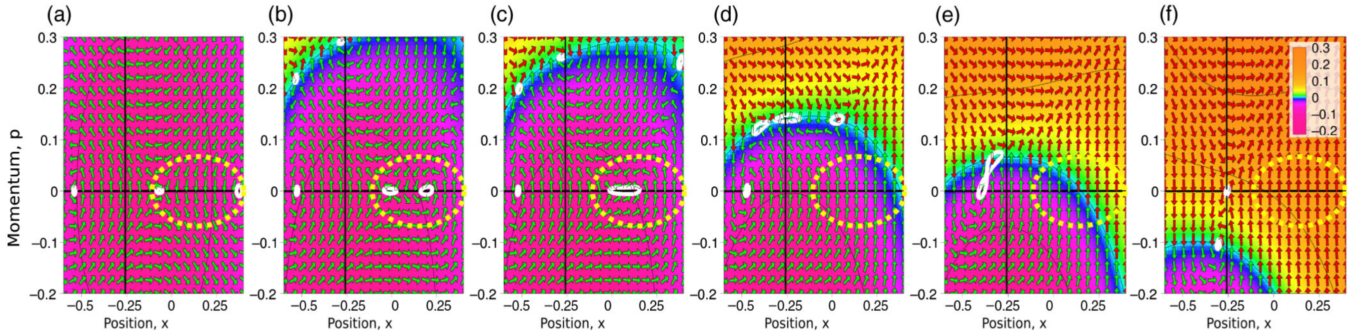

FIG. 5 (color online). Same system parameters as for Fig. 2: Contour plots of Wigner function with superimposed normalized flow field $\boldsymbol{J}/|\boldsymbol{J}|$ at times $t = 0, 0.075T, 0.0875T, 0.15T, 0.2T$, and $0.325T$ in panels **a** to **f** demonstrates mergers and splitting of stagnation points and their pinning to zeros of the Wigner function. Each vertical black line shows the position X_S of the tunnelling barrier top. Small white loops delineate areas where $\boldsymbol{J}^2 = 2 \times 10^{-6}$ and encircle stagnation points. We chose the region where the torus closes and several stagnation points coalesce (compare Fig. 4). The cross sections of the torus are visible in the right half of panels (a), (b), and (c), a convex loop $\mathcal{L}$ encircling both torus points only, such as the dotted yellow ellipse, yields $\omega = 0$. This value is conserved over time throughout the merger which leads to the disappearance of the torus [panel (d)]. The mergers of the four stagnation points outside the yellow loop (two vortices and two separatrix crossings) in panels (d), (e), and (f) into one vortex and one separatrix crossing evidently carry a conserved total topological charge of zero throughout.

Fig. 2(b). The further apart the two wells, the finer the interference pattern [10] and the stronger the resulting flow cancellation. Thus we find that tunneling can be described as a transport phenomenon that plays out over large parts of quantum phase space [6,25], frustrated by phase space interference.

For a low energy state, such as Ψ, the positions of remnant vortices originating from the potential's minima positions are quantum displaced inward, towards the potential barrier, Figs. 3 and 4.

In classical physics stagnation points of phase space flow can only occur on the x axis, here, according to Eq. (2), they are pinned to the zero lines of the Wigner function, but occur off the x axis, travel long distances and merge with or split from other stagnation points, see Figs. 4 and 5.

For the Caticha potential, we observe a string of vortices with alternating handedness aligned in the p direction located near the top of the tunnelling barrier, at position $X_S = -0.258$, Fig. 3. Over time they travel in the negative p direction, Figs. 4 and 5. When reaching the x axis they coalesce with the remnant separatrix intersection point while the overall topological charge of the flow is conserved; see Fig. 5.

To conclude, Wigner flow reveals nonclassical features and added complexity of quantum phase space dynamics. At the same time it provides, through the conservation of the flow winding number ω, the basis for an analysis of its topological invariants, ordering this complexity.

Systems that have been studied using quantum phase space techniques can be analyzed using Wigner flow. Such systems arise [17], for example, in chemical quantum dynamics [13,14,26], "nonlinear" quantum processes in closed single particle [15] or open multiparticle [27–29] systems, classical electromagnetic fields [30], and multiband semiconductor physics [31].

Use of the high-performance computing facility at the University of Hertfordshire's Science and Technology Research Institute is gratefully acknowledged. We thank Charles Young, Elias Brinks, Daniel Polani, Andreas Kukol, and Cosmas Zachos for comments on the manuscript.

*O. Steuernagel@herts.ac.uk

[1] D. D. Nolte, Phys. Today **63**, No. 04, 33 (2010).
[2] M. V. Berry, in *Regular and Irregular Motion*, AIP Conf. Proc. No. 46 (AIP, New York, 1978).
[3] A. Donoso, Y. Zheng, and C. C. Martens, J. Chem. Phys. **119**, 5010 (2003).
[4] H. Bauke and N. R. Itzhak, arXiv:1101.2683v1.
[5] In degenerate quantum cases flow reversal can occur but none of the other nonclassical flow patterns listed here.
[6] R. T. Skodje, H. W. Rohrs, and J. Vanbuskirk, Phys. Rev. A **40**, 2894 (1989).
[7] E. Wigner, Phys. Rev. **40**, 749 (1932).
[8] M. Hillery, R. F. O'Connell, M. O. Scully, and E. P. Wigner, Phys. Rep. **106**, 121 (1984).
[9] W. P. Schleich, *Quantum Optics in Phase Space* (Wiley-VCH, New York, 2001).
[10] W. H. Zurek, Nature (London) **412**, 712 (2001).
[11] P. Grangier, Science **332**, 313 (2011).
[12] A. Ferraro and M. G. A. Paris, Phys. Rev. Lett. **108**, 260403 (2012).
[13] A. Donoso and C. C. Martens, Phys. Rev. Lett. **87**, 223202 (2001).
[14] K. H. Hughes, S. M. Parry, G. Parlant, and I. Burghardt, J. Phys. Chem. A **111**, 10 269 (2007).
[15] O. Gat, J. Phys. A **40**, F911 (2007).

[16] J. S. Bell, *Speakable and Unspeakable in Quantum Mechanics. Collected Papers on Quantum Philosophy* (Cambridge University Press, Cambridge, England, 1987).
[17] *Quantum Mechanics in Phase Space*, edited by C. K. Zachos, D. B. Fairlie, and T. L. Curtright (World Scientific, Singapore, 2005), Vol. 34.
[18] O. Steuernagel, arXiv:1008.3929.
[19] C. Kurtsiefer, T. Pfau, and J. Mlynek, Nature (London) **386**, 150 (1997).
[20] M. R. Dennis, K. O'Holleran, and M. J. Padgett, in *Progress in Optics*, edited by E. Wolf (Elsevier, New York, 2009), Vol. 53, p. 293.
[21] A. Caticha, Phys. Rev. A **51**, 4264 (1995).
[22] See Supplemental Material at http://link.aps.org/supplemental/10.1103/PhysRevLett.110.030401 for the Wigner flow patterns of states ψ_0 and ψ_1.
[23] To determine the Wigner functions we integrated y from $-2.7, \dots, 2.7$. The summation cutoff for the determination of J_p was chosen at $l_{\max} = 12$.
[24] M. V. Berry and N. L. Balazs, J. Phys. A **12**, 625 (1979).
[25] N. L. Balazs and A. Voros, Ann. Phys. (N.Y.) **199**, 123 (1990).
[26] L. L. Gibson, G. C. Schatz, M. A. Ratner, and M. J. Davis, J. Chem. Phys. **86**, 3263 (1987).
[27] B. M. Garraway and P. L. Knight, Phys. Rev. A **50**, 2548 (1994).
[28] I. Katz, R. Lifshitz, A. Retzker, and R. Straub, New J. Phys. **10**, 125023 (2008).
[29] S. Rips, M. Kiffner, I. Wilson-Rae, and M. J. Hartmann, New J. Phys. **14**, 023042 (2012).
[30] M. Levanda and V. Fleurov, Ann. Phys. (N.Y.) **292**, 199 (2001).
[31] O. Morandi, Phys. Rev. B **80**, 024301 (2009).